PROCEEDINGS OF SCIENCE

QCD phase diagram constructed with effective models

Carline Biesdorf,[a,*] **Luiz L. Lopes**[b] **and Debora P. Menezes**[a]

[a] *Departamento de Física, CFM - Universidade Federal de Santa Catarina, C.P. 476, CEP 88.040-900, Florianópolis, SC, Brasil*

[b] *Centro Federal de Educação Tecnológica de Minas Gerais Campus VIII, CEP 37.022-560, Varginha, MG, Brasil*

E-mail: carline.fsc@gmail.com

In this work, we obtain a representation of the QCD phase diagram with the help of two effective models, MIT based bag models to describe quark matter and QHD based models to describe hadronic matter. To obtain the phase transition line, we use the Gibbs conditions that determine the critical chemical potential for symmetric matter at zero and finite temperature.

XV International Workshop on Hadron Physics (XV Hadron Physics) 13 -17 September 2021
Online, hosted by Instituto Tecnológico de Aeronáutica, São José dos Campos, Brazil

*Speaker

PoS(XVHadronPhysics)035

1. Effective models

To describe hadronic matter we use an extension of the Quantum Hadrodynamics (QHD) with non-linear terms. The Lagrangian density reads:

$$\begin{aligned}\mathcal{L}_{NLWM} = &\sum_N \overline{\psi}_N[\gamma_\mu(i\partial^\mu - g_\omega\omega^\mu - g_\rho\vec{\tau}_N\vec{\rho}^\mu - M_N^*]\psi_N + \frac{1}{2}\partial_\mu\sigma\partial^\mu\sigma - \frac{1}{2}m_\sigma^2\sigma^2 \\ &- \frac{1}{3!}\kappa\sigma^3 - \frac{1}{4!}\lambda\sigma^4 - \frac{1}{4}\Omega^{\mu\nu}\Omega_{\mu\nu} + \frac{1}{2}m_\omega^2\omega_\mu\omega^\mu + \frac{1}{4!}\xi g_{N\omega}^4(\omega_\mu\omega^\mu)^2 \\ &- \frac{1}{4}\vec{R}_{\mu\nu}\vec{R}^{\mu\nu} + \frac{1}{2}m_\rho^2\vec{\rho}_\mu\vec{\rho}^\mu + \Lambda_v g_{N\omega}^2 g_{N\rho}^2\omega_\mu\omega^\mu\vec{\rho}_\mu\vec{\rho}^\mu, \end{aligned} \tag{1}$$

where the Dirac spinor ψ_N represents the two nucleons with the effective mass $M_N^* = M_N - g_\sigma\sigma$ and isospin $\vec{\tau}_N$. The m_i's and the g_i's are, respectively, the mass of the meson i ($i = \sigma, \omega, \rho$), and the coupling constants of the mesons with the nucleon N. Applying the mean field approximation (MFA), the EoS can be obtained from eq. (1) (see ref. [1]).

We choose two parametrizations: L3$\omega\rho$ [2] and FSU2H [3] that satisfy bulk nuclear matter properties and also reproduce maximum star masses above 2M$_\odot$ even when hyperons are included.

To describe quark matter we choose two different approaches. The first one uses the original MIT bag model and the second is a modification of that model with the inclusion of a vector field, as presented in [4]. The Lagrangian density of the model follows:

$$\mathcal{L}_{MIT} = \sum_q \left\{\overline{\psi}_q\Big[\gamma^\mu(i\partial_\mu - g_V V_\mu) - m_q\Big]\psi_q + \frac{1}{2}m_V^2 V_\mu V^\mu - B\right\}\Theta(\overline{\psi}_q\psi_q) - \frac{1}{2}\overline{\psi}_q\psi_q\delta_S, \tag{2}$$

where the Dirac spinor ψ_q represents the quark with mass m_q, g_V the coupling constant, and m_V the mass of the meson. Using mean field approximation we obtain the EoSs as shown in ref. [4].

We choose two values for the bag pressure: $B^{1/4} = 148$ MeV, which is the lowest value within the stability window [4] that satisfies the Bodmer-Witten conjecture, and $B^{1/4} = 163$ MeV, which is outside the stability window. In order to obtain higher transition temperatures at low chemical potentials, we here also consider a temperature dependent bag model, as done in [5]:

$$B(T) = B_0\left[1 + \left(\frac{T}{T_0}\right)^4\right], \tag{3}$$

where T_0 is adjusted to reproduce the LQCD and freeze-out (pseudo) critical temperature at zero chemical potential. Thus we use $T_0 = 131$ MeV for $B_0^{1/4} = 148$ MeV and $T_0 = 152$ MeV for $B_0^{1/4} = 163$ MeV.

2. First order phase transition - Gibbs conditions - and flavor conservation

The criteria we use to calculate the phase transition are the Gibbs conditions [6]:

$$T^{(H)} = T^{(Q)} = T, \qquad P^{(H)} = P^{(Q)} = P_0, \qquad \mu^{(H)}(P_0, T) = \mu^{(Q)}(P_0, T) = \mu_0, \tag{4}$$

with

$$\mu^{(f)} = \frac{\epsilon^{(f)} + P^{(f)} - s^{(f)}T}{n_B^{(f)}}, \tag{5}$$

where $\epsilon^{(f)}$, $P^{(f)}$, $s^{(f)}$ and $n_B^{(f)}$ are the total energy density, pressure, entropy density and number density of the phase $f = \{H, Q\}$.

Now, once the time scale of the strong force is very small, we consider flavor conservation during the phase transition, so that the quark phase is completely determined from the initial hadronic matter. As we have symmetric matter for the hadronic phase, we also must have symmetric matter for the quark phase.

In Fig. 1 we show examples where the Gibbs conditions are satisfied for $T = 120$ MeV and $T = 0$.

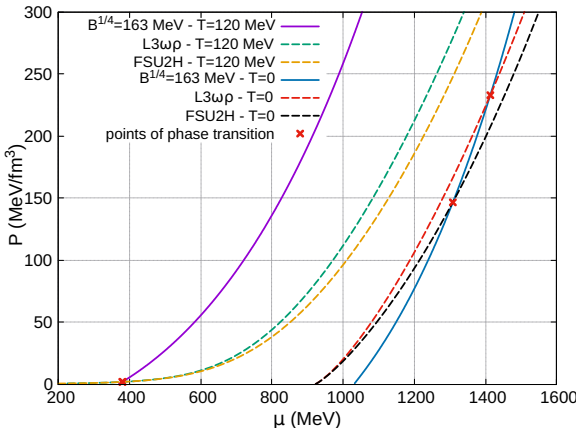

Figure 1: Relation between pressure and chemical potential for the hadron (dashed lines) and quark (solid lines) phases, respectively described by the L3$\omega\rho$ and FSU2H parametrization and $B^{1/4} = 163$ MeV considering $T = 120$ MeV and $T = 0$. The red dots are the points where the Gibbs conditions are satisfied.

3. Phase Diagrams

In Fig. 2 we present the phase diagrams obtained considering two-flavored symmetric matter for both phases. Also, for sake of completeness, we display the phase diagram for pure quark matter using MIT based models. In this case, the phase transition criteria is just the value of the chemical potential where the pressure goes to zero. At the top figures, the bag pressure values are constant. In this case, the maximum critical temperature obtained for low chemical potentials, depends solely on the value of the $B^{1/4}$, i.e., for a fixed $B^{1/4}$ value, different parametrizations for the hadronic phase or even the inclusion of a vector field to the MIT bag model do not change the value of the maximum temperature. Hence we draw the same conclusion as in [5]: the bigger the $B^{1/4}$ value the higher the maximum temperature. To understand this behavior we take a look at the relation $\mu \times P$ at high temperatures. As can be seen in Fig. 1, the crossing of the curves from the two phases occurs at very low pressures. So, as the condition to phase transition used when considering only

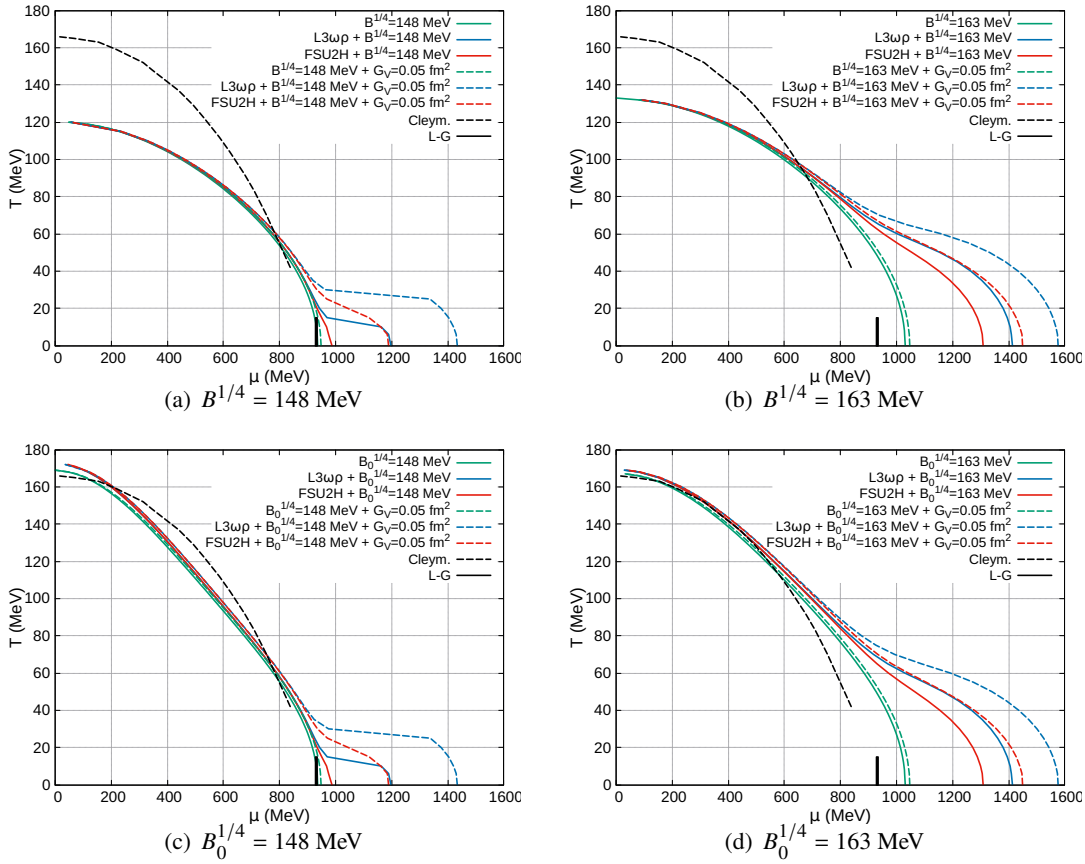

(a) $B^{1/4}$ = 148 MeV (b) $B^{1/4}$ = 163 MeV

(c) $B_0^{1/4}$ = 148 MeV (d) $B_0^{1/4}$ = 163 MeV

Figure 2: Phase diagrams for symmetric matter considering the L3$\omega\rho$ and FSU2H parametrizations for the hadronic matter and two different MIT based bag models for two constant $B^{1/4}$ values (top) and two temperature-dependent bag $B(T)$ (bottom) for the quark matter. The Cleym. line is the experimental freeze-out [9] and L-G is the region where we expect a liquid-gas phase transition [10].

the MIT bag model is $P = 0$, it is not surprising that the results at this region of the phase diagram all coincide.

At higher chemical potentials, however, the influence of the hadronic phase shows up, so that the line of coexistence distances itself from the line obtained via MIT based model only. The inclusion of a vector field to the MIT bag model increases the critical chemical potential, as already stated in [5], but here this influence is increased as can be seen by comparing the solid line with the dashed line of the same color. The differences for the critical chemical potentials between different QHD parametrizations for a fixed bag value also increase when the bag value is higher. The $L3\omega\rho$ parametrization results in a higher critical chemical potential than the FSU2H parametrization. In the same way, vector MIT based models produce a higher critical chemical potential. This is related with the stiffness of each model. A stiffer QHD model produces a lower critical chemical potential when compared with a softer one. One has to bear in mind that this feature depends on the region where the crossing of the curves takes place since FSU2H is stiffer than L3$\omega\rho$ only up to a certain density (around 0.65 fm^{-3}). On the other hand, for the quark phase we have two behaviors. When we increase the bag pressure value, which softens the EoS, we obtain higher chemical potentials.

But when we include the vector channel, which, in turn, stiffens the EoS, we also increase the chemical potentials. To a more profound discussion, see [7].

With constant bag pressure values we are not able to obtain maximum temperatures that satisfy the constrains imposed by LQCD [8] nor the freeze-out results [9] and so we are not able to fit the Cleymans line entirely inside the confined (hadron) phase (see ref. [9]). So, we make use of temperature-dependent bag pressure values. The results are presented at the bottom of Fig. 2. As can be seen, we are only able to fit the Cleymans line entirely inside the confined (hadron) phase for the combinations that includes a $B_0^{1/4} = 163$ MeV and any of the QHD based model. In fact, $B_0^{1/4} = 163$ MeV is the smallest value that allows us to satisfy this constrain. We can also see that a phase diagram constructed using MIT based model alone always produces a lower value of the maximum chemical potential when compared with a phase diagram that uses both, a QHD and a MIT based model.

4. Conclusions

In this work, we sought to obtain a representation of the QCD phase diagram using two effective models, MIT based bag models and QHD based models. We were only able to fulfill the constraints imposed by LQCD [8] and freeze-out results [9] using a temperature-dependent bag pressure with $B_0^{1/4} = 163$ MeV and any one of the QHD based models presented. However, if we also impose that the maximum critical chemical potential has to lie between $1050 < \mu < 1400$ MeV, as discussed in [5], only a combination with the FSU2H fulfils all constraints.

Acknowledgments: This work is a part of the project INCT-FNA Proc. No. 464898/2014-5. D.P.M. was partially supported by Conselho Nacional de Desenvolvimento Científico e Tecnológico (CNPq/Brazil) under grant 303490-2021-7 and C.B. acknowledges a doctorate scholarship from Coordenação de Aperfeiçoamento de Pessoal do Ensino Superior (Capes/Brazil).

References

[1] B. Serot, Reports on Progress in Physics **55**, 1855 (1992).

[2] L. Lopes, Communications in Theoretical Physics **74**, 015302 (2021).

[3] L. Tolos, M. Centelles, and A. Ramos, Publications of the Astronomical Society of Australia **34** 34 (2017)

[4] L. Lopes, C. Biesdorf, and D. Menezes, Physica Scripta **96**, 065303 (2021).

[5] L. Lopes, C. Biesdorf, K. Marquez, and D. Menezes, Physica Scripta **96**, 065302 (2021).

[6] I. Bombaci, I. Parenti and I. Vidana, The Astrophysical Journal. **614**, 314 (2004)

[7] L. Lopes, D. Menezes, Nuclear Physics A, **1009**, 122171 (2021)

[8] A. Bazavov et al., Physical. Review. D **96**, 074510 (2017)

[9] J. Cleymans, et al., Physical Review C **73**, 034905 (2006).

[10] J. Finn, et al., Physical Review Letters **49**, 1321 (1982).